A Wavelet-Predominant Algorithm Can Evaluate Quality of THz Security Image and Identify Its Usability

Menghan Hu, Guangtao Zhai, *Member, IEEE*, Rong Xie, Xiongkuo Min, Qingli Li, Xiaokang Yang, *Fellow, IEEE*, and Wenjun Zhang, *Fellow, IEEE*

***Abstract*—This paper presents an aggregate wavelet-predominant algorithm to measure the distortions in THz security images. The algorithm integrates a spectral-based sharpness estimator, a noise estimator derived alpha-stable model and an overall viewing experience estimator based on free-energy principle. Among them, the greater weight is assigned to the spectral-based sharpness estimator considering that the main quality factor in THz security image is sharpness. To verify the feasibility of the proposed metric, we construct the THz security image dataset including a total of 181 THz security images, and each image has the mean opinion score (MOS) collected via subjective quality evaluation experiment. Quantitative experimental results on the constructed THz security image dataset show that the aggregate wavelet-predominant estimator produces the promising overall performance for the estimation of MOS values, with PLCC, SROCC, and RMSE of 0.900, 0.873, and 0.386, respectively. This performance is superior to other opinion-unaware approaches, *viz.*, FISBLIM, SISBLIM, NIQE, CPBD, SINE, S3, FISH, and noise estimator. The determination coefficient (R^2) of linear regression between reference and predicted MOSs is 0.81. The result of Bland–Altman analysis further validates that the aggregate wavelet-predominant estimator can substitute for the subjective IQA of THz security image, with approximately 94.5% of data points locating within the limits of agreement. For usability identification, the wavelet-predominant estimator gives the satisfactory results, with accuracy, precision, recall rate, and false positive rate of 84.0%, 79.8%, 95.0%, and 29.6%, respectively. Furthermore, the potential application perspectives of the proposed metric can refer to commercial applications (guarantee THz security images of good quality) and scientific researches (assist in software development for THz security image analysis). The dataset is available at https://doi.org/10.6084/m9.figshare.7700123.v3. Possible researches on this dataset may include the development of THz quality standards, the selection of the best display mode, the enhancement of images, the modeling of image noise, and the detection of prohibited goods.**

***Index Terms*—Terahertz security image dataset, usability identification, blind image quality assessment, free-energy principle, alpha-stable distribution.**

I. Introduction

TERAHERTZ (THz) radiation lies roughly in the frequency gap between the infrared (30 GHz) and microwaves (300 GHz) [1]. This band was once called THz gap, because no semiconductor technology could be used to efficiently convert electrical power into electromagnetic radiation in this waveband at that time [2]. Due to the ongoing advances in photonics and nanotechnology, the past 20 years have witnessed an unprecedented development of THz science and technology [3]. Spurred by the powerful ability of THz imaging technique for acquisition of valuable data, it has been widely applied as an analytical tool in both basic and applied research domains [4]. For instance, Moldosanov *et al.* validated a potential of THz imaging technique as a non-invasive technique for detection of pathological modifications of cancer in human organs [5]. In terms of security application, compared to the other imaging techniques such as X-ray imaging, THz imaging technique has three prominent merits [6], [7]: (1) exists no radiation hazard for scanned people; (2) is able to detect non-metallic and non-polar materials; and (3) has capability of identifying explosives and illicit drugs.

In spite of the advantages of THz imaging technique such as low photon energy and high transparency, most existing THz imaging devices are equipped with low-stability sources at insufficient power levels and conduct one scan with several seconds. For this reason, the quality of obtained THz image is extremely influenced by the variations of environmental factors inclusive of temperature and humidity [8]. In addition, the instable performance of imaging equipment deteriorates the quality of final THz image. These will further reduce the usability of ultimate THz image. To extend THz imaging technique to larger scale applications, a corresponding strategy is urgently needed to evaluate the quality and identify the usability of THz security image.

Image quality assessment (IQA) offers an efficient solution to quantitatively evaluate quality of THz security image and identify its usability, thus allowing the subsequent

Manuscript received October 30, 2018; revised February 2, 2019; accepted February 7, 2019. This work was supported in part by the Shanghai Sailing Program under Grant 19YF1414100, in part by the National Natural Science Foundation of China under Grant 61377107, Grant 61831015, and Grant 61527804, in part by the Science and Technology Commission of Shanghai Municipality under Grant 18511102500, and in part by the Equipment Pre-research Joint Research Program of Ministry of Education under Grant 6141A020223. *(Corresponding author: Rong Xie.)*

M. Hu and Q. Li are with the Shanghai Key Laboratory of Multidimensional Information Processing, East China Normal University, Shanghai 200062, China.

G. Zhai, R. Xie, X. Min, X. Yang, and W. Zhang are with the Institute of Image Communication and Information Processing, Shanghai Jiao Tong University, Shanghai 200240, China (e-mail: xierong@sjtu.edu.cn).

Color versions of one or more of the figures in this paper are available online at http://ieeexplore.ieee.org.

Digital Object Identifier 10.1109/TBC.2019.2901388

improvement of detection or prediction accuracies [9]. IQA is of great significance for numerous image and video processing tasks, whose objective is to automatically examine image quality in agreement with human quality judgments [10] or task requirements. IQA can be divided into subjective IQA and objective IQA. The subjective IQA is inconvenient, expensive and time-consuming, but it is still considered as an effective means to assess image quality [11]. The objective IQA reflects the subjective perception using a mathematical model, and gives a judgement or prediction based on numerical calculations. The current objective IQA methods are generally classified into three categories, viz. full-reference, reduced-reference and no-reference or blind approaches, depending on the accessibility of reference images [12]. On account of the difficulties to capture and define perfect reference THz images in the real-world THz imaging procedure, the no-reference IQA algorithms are recommended for quality evaluation and usability identification of THz security image. It is noteworthy to contemplate subcategories of general-purpose no-reference IQA models having tighter conditions [13]: (1) opinion-aware no-reference model: the model has been trained on human rated distorted images and associated subjective opinion scores. The algorithms including NFERM [14], GMLF [15], DIIVINE [16], BRISQUE [17] and BLIINDS2 [18] belong to this category. For fairness, we do not choose these methods for subsequent comparisons; and (2) opinion unaware no-reference model: the model does not require training on databases of human judgments of distorted images, only requires knowledge of the expected image distortions. For THz image quality evaluation, the algorithm we developed is without any training procedures, and it belongs to the opinion unaware no-reference approach.

With respect to usability identification of THz security image, the IQA indicator can be regarded as a criterion for judging whether the obtained THz security images meet specific application requirements. Image usability identification is not equivalent to image quality evaluation but can be regarded as an improvement and deepening of image quality evaluation concept. In the framework of image usability identification, the core concept involved is the maximum allowable distortion. This is a relatively new concept, and the opposite concept is the just noticeable difference in psychological research. Fig. 1 shows a closed cycle which demonstrates the role of usability identification in THz security application. Compared to the quality evaluation, scientists should pay more attention to usability identification of THz security image, because such operation has capability of assisting in improving the performance of imaging system, optimizing image acquisition and processing modules, and monitoring the working conditions of imaging components.

IQA has been widely applied for usability identification of natural images. However, it is rarely used for usability identification of images in specific modalities. For usability identification of medical image, Chow and Paramesran summarized the IQA algorithms for magnetic resonance image, computed tomography and ultrasonic image [19]. In security applications, the usability of obtained image plays a very important role in illegal items screening. Five image features containing sharpness, brightness, resolution, head pose and facial expression were leveraged by Long and Li to assess the usability of near infrared face image [20]. The effectiveness of their approach was validated in a near infrared database established by Center for Biometrics and Security Research. Wu *et al.* developed an IQA software based on statistics and analysis of pixel number and gray level value of region of interest [21]. The experimental results demonstrated that the decision derived by IQA software was consistent with that by operators perception. Irvine *et al.* conducted a similar research, who used image quality metrics extracted from actual X-ray data to estimate the perceived quality of X-ray image [22]. The linear model established in their study can predict the image quality score with R^2 of 0.834. Galbally *et al.* utilized a total of 25 general IQA metrics for fake biometric detection [23]. The experimental results, acquired on publicly available data sets, showed a potential ability of IQA metric for identification of real and fake biometrics. Some other investigators carried out similar work [24], [25]. For THz image, Hou *et al.* computed mean square error of the peak values of time domain in a columns pixel to evaluate THz image quality [8]. Fitzgerald *et al.* computed a modulation transfer function from an amplitude of optical transfer function to verify the spatial resolution of THz image [9]. Our research group had presented a preliminary result, which used 5 opinion-aware and 8 opinion-unaware approaches to estimate noise level of THz image [26]. To the best of our knowledge, apart from above three publications, there is no other related work with respect to usability identification of THz image using IQA.

Thus, the objectives of the current work are to: (1) construct the THz security image dataset and give the corresponding mean opinion scores (MOSs) for each image based on the specific subjective evaluation criterion; (2) develop a wavelet-predominant metric without any training procedures to evaluate quality of THz security image and compare its performance to the existing opinion unaware no-reference IQA algorithms; and (3) use the IQA metrics of good performance to identify the usability of THz security image and discuss the signicance of IQA approach in the development of THz imaging technique and THz image analysis software.

II. Visual Quality Perception Experiment of THz Security Image

A. THz Imaging Equipment

In the current work, THz security images are obtained via the active THz reflectance imaging device (Fig. 2). THz wave is generated by a THz wave generator and then the interacted signals are recorded by a THz wave detector. Both THz wave generator and its detector are assembled on a plate located at the same side of testing person. The detection space is divided into 200 subsections, and the THz detector is used to capture the THz reflectance signals on all subsections. The THz device used in this study is a research device developed by BOCOM Smart Network Technologies Inc.

The imaging parameters of the THz device are listed below: the effective scanning volume:

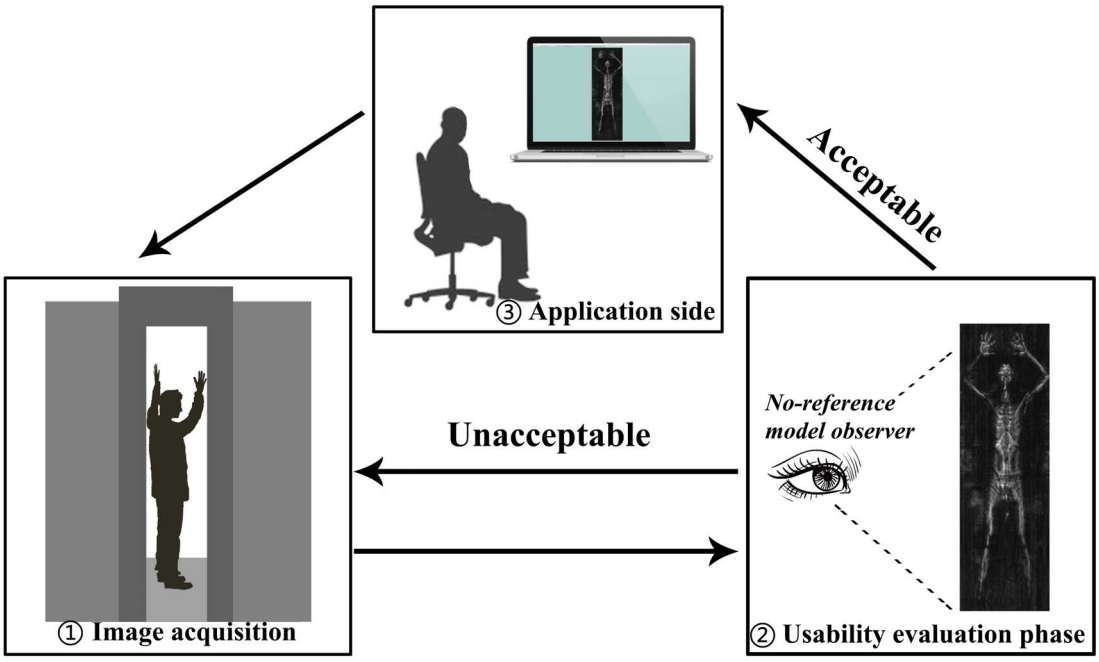

Fig. 1. A closed cycle demonstrating role of usability identification in THz security application.

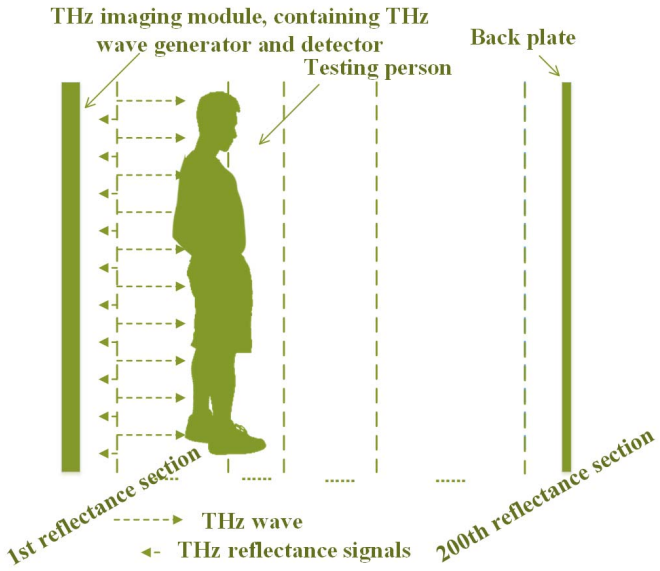

Fig. 2. The operating principle of active THz reflectance imaging device.

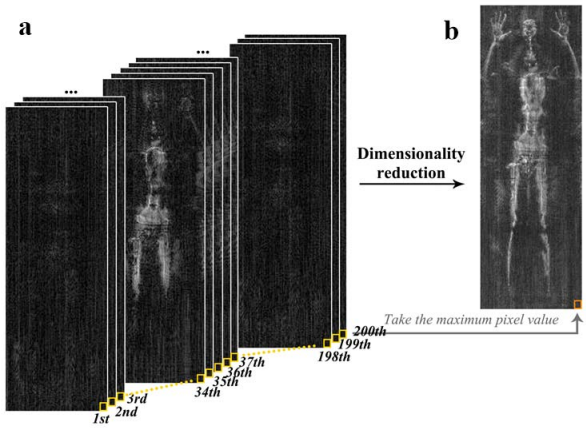

Fig. 3. One THz image sample demonstrating data transformation: (a) three-dimensional THz image cube, and (b) two-dimensional THz image.

0.15m-2.00m(height)× ≈1.00m(length)× ≈1.00m(width); scanning time<3 seconds; type of imaging device: custom-made Transmit/Receive (T/R) module which operates in active reection imaging mode; resolution: line resolution×spatial resolution=(<2mm)×(<6mm).

B. Description of THz Security Image Dataset

To generate the dataset, four volunteers were invited to stand in the THz imaging device, and imaged with various legal goods such as bracelet or illegal substances such as hammer each time. For more information, please refer to the dataset we released(https://doi.org/10.6084/m9.figshare.7700123.v3).

Based on the THz imaging principle, the raw THz image is a three-dimensional image cube (Fig. 3 (a)). A two-dimensional THz image (Fig. 3 (b)) used in following analysis can be formed by combining the maximum pixels in the Z direct into a new two-dimensional plane from a three-dimensional THz image cube. The eventual THz security image dataset is composed of 181 THz images with a resolution of 127×380.

C. Distortions in THz Security Image

Before the subjective experiments, two main distortions in THz image are clarified, which are noise and blur distortions. The noise type for THz image contains the sensor noise and non-uniformity noise. The sensor noise may be generated by light sensitivity based on the integration times of THz sensor. The non-uniformity noise is conspicuous in THz security image and it is an additive fixed-pattern noise, appearing as a

Fig. 4. One THz image example for the analysis of main distortion type in THz security images. (Red circle and rectangles are applied for highlighting the illegal target and ripple noises respectively).

ripple or striping pattern. The non-uniformity noise, resulting from the unstable imaging device and changeable experimental factors, makes the unlawful materials unidentified by human eyes or imaging processing algorithms. The blur distortion, one of structural distortions, occurs when the volunteer shakes during the image acquisition, and it is indeed deteriorates THz security image quality. From the above analysis, the noise and blur distortions are considered as two major factors which seriously decrease the usability of THz image. For human eye, the blur in the THz security image is easier to perceive and affects the human viewing experience. Hence, blurriness (the antonym of sharpness) is considered as the main distortion in THz security image.

Fig. 4 shows one THz image with the volunteer taking phone in the right pocket, and the ripple noises caused by the unstable imaging device and changeable experimental factors make this target to be detected unidentied by human eyes or imaging processing algorithms.

D. Subjective Evaluation of THz Image Quality

There is no corresponding subjective evaluation framework for THz security image. After the communication with the experts and engineers in THz research domain, we design a subjective image quality assessment experiment based on a double-stimulus method according to ITU BT.500 [27]. After the experiment, the mean opinion scores (MOSs) of THz security images can be obtained by the following equation:

$$MOS_j = \sum_{i=1}^{N} u_{i,j}/N_i \tag{1}$$

where N_i and $u_{i,j}$ denote the number of observers and the score of image j assigned by the ith observer, respectively.

For the subjective experiment, the objective and procedure of the experiment were individually introduced to all observers in detail. The experiment was conducted under the normal indoor illumination of about 2400 Lux. The illumination intensity of the testing room was monitored by the digital light meter (TA8131, TASI ELECTRONIC CO.,LTD., Jiangsu, PR China). The testing images were displayed in the 23 inches LED monitor with a resolution of 1920×1080, and the viewing distance was set to 2-2.5 screen heights. The subjective evaluation criterion below is presented for subjective experiments.

TABLE I
SUBJECTIVE EVALUATION CRITERION USING FIVE-GRADE SCALE FOR THZ IQA

Score	Quality	Standard
5	Excellent	Acceptable
4	Good	Unacceptable, but not annoying
3	Fair	Slightly annoying
2	Poor	Annoying
1	Bad	Quite annoying

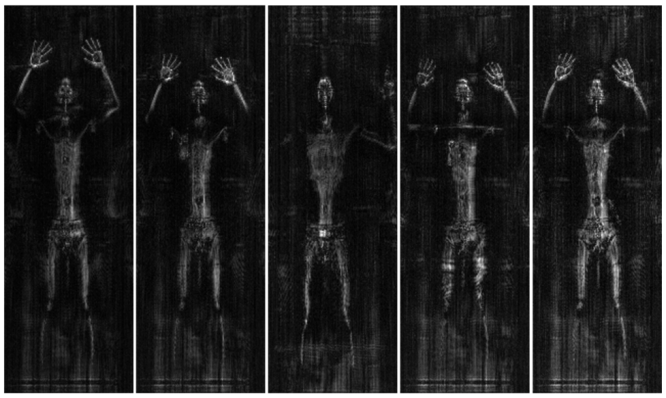

Fig. 5. Five reference THz security images for each grade presented in Table I.

In the double-stimulus experiment, the corresponding reference THz images of each quality grade (Fig. 5) were chosen by two experts who were exclusive of subjective experiment. Subsequently, a total of fifteen observers including two experts and thirteen subjects having no related expertise were recruited to assess the quality of THz security images. All the observers were asked to give their score mainly considering subjective evaluation criteria of five-grade scale.

E. Definition of THz Image Usability

Based on the above analysis, a MOS vector can be obtained. Fig. 6 demonstrates the statistical histograms of this vector.

The THz security images whose MOSs are below and up 3 are divided into the usable and unusable categories, respectively. What we are more concerned with is that whether the THz security image quality can meet the inspectors acceptability or final applicable requirements in real-world applications. The experts select reference images based on the following criteria: quality score=5: the structure of human body is very clear and there is almost no noise; quality score=4: the structure of human body is clear and the level of overall noise is acceptable; quality score=3: the structure of human body is somewhat blurry and confuses with noise; quality score=2: the structure of human body is blurry and confuses with noise; quality score=1: the structure of human body is blurry, confuses with noise, and the level of overall noise is unacceptable.

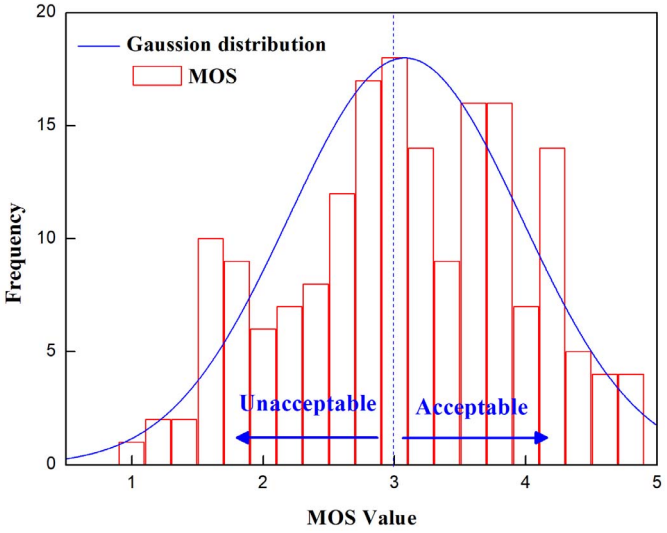

Fig. 6. Statistical distributions of MOS values for THz security images. (The vertical dotted lines are used to divide THz images into usable and unusable categories).

According to the suggestion of inspectors, when the quality score is less than 3, most contraband goods are difficult to be recognized by the naked eyes and viewing these images may cause inspectors uncomfortable and even annoyed. Hence, the definition of THz security image usability U is:

$$U = \begin{cases} Acceptable, & MOS_j \geq 3 \\ Unacceptable, & MOS_j < 3 \end{cases} \tag{2}$$

A total of 100 and 81 images are classified into acceptable and unacceptable categories respectively. Subsequently, a k-means clustering algorithm, an unsupervised classification approach, is used to classify the THz security images as the acceptable and unacceptable categories.

III. A Wavelet-Predominant Algorithm

In this section, we describe the operation of the wavelet-predominant algorithm for THz security images, an outline of which is shown in Fig. 7. There exist noise and blur distortions in THz images, and subsequently, some subjective visual experience will be introduced during the subjective image quality assessment experiments. Therefore, as shown in Fig. 7, three estimators are employed: 1) a spectral-based sharpness estimator, which was first proposed by Phong and Damon [28] (FISH, Fast Image Sharpness); 2) a noise estimator, which operates based on an alpha-stable model [29]; and 3) an overall viewing experience estimator, which is characterized by a free energy principle [14], [30]. The final estimator for characterizing the distortion of THz security image is computed by combining these three estimators.

A. Spectral-Based Sharpness Estimator (FISH, Fast Image Sharpness)

Given a THz security image I, the Cohen-Daubechies-Feauveau 9/7 wavelet transform [31] is applied to conduct the three-level decomposition for the THz security image I. Fig. 8 demonstrates the results of three-level separable discrete wavelet transform (DWT) for image I.

To quantify the high-frequency content in the THz security image I, the log-energy of S_{xy} is calculated using the equation below:

$$E_{xy_n} = \log_{10}\left(1 + 1/N_n \sum_{i,j} S^2_{xy_n}(i,j)\right) \tag{3}$$

In this equation, S_{xy} denotes the sub-bands at the DWT level $n \in [1, 2, 3]$ with the exception of LL_3 sub-band ($xy \in [LH, HL, HH]$); N_n is the number of DWT coefficients in each sub-band at decomposition level n; and (i, j) is the coordinates for each pixel. The total log-energy can be computed via the following equation:

$$E_n = \big((1-\alpha)\big(E_{LH_n} + E_{HL_n}\big)/2\big) + \alpha E_{HH_n} \tag{4}$$

where α is an empirical value. Because the HH band is considered to span a higher radial spatial frequency than the LH and HL bands, 0.8 is assigned to α to let the HH band have the greater weight in E_n. The overall sharpness estimator can be obtained as follows:

$$FISH = \sum_{n=1}^{3} 2^{3-n} E_n \tag{5}$$

FISH has been validated in the quality estimation of natural images [28]. It has been also validated by us and is valid in the quality estimation of THz security images.

B. Noise Estimator for THz Security Image

It has been found in [29] that an alpha-stable distribution can be utilized to fit the noise of THz image instead of the commonly-used Gaussian distribution owing to the special attributes of the THz image compared with the natural image. According to the special attributes of distortions in THz security image (Fig. 4), the calculation of noise estimator is composed of the following three steps.

Step 1: Extraction of non-salient regions: Let I_s and I_{ns} respectively denote the salient region and the non-salient region of image I. We extract I_s of a THz security image I using the Graph-Based Visual Saliency (GBVS) algorithm [32]. Before the saliency detection, the resolution of image I is resized from 127×380 to 128×380 to meet the requirement of GBVS algorithm. The pixels of human gaze and background area of I_s are set as 1 and 0 to form the binary image I_{bs}. Then, I_{ns} is generated via

$$I_{ns} = a_{i,j} \times b_{i,j}, \;\; a_{i,j} \in I_{bs}, b_{i,j} \in I \tag{6}$$

The result of this procedure is shown in Fig. 9 (a).

Step 2: Determination of valid image block: Because noise in background region is stripy, we divide the image I into 152 blocks, and the size of each block is 20×16 (Fig. 9 (b)). Based on the imaging principle, there is no pixel equal to 0 in the original THz images. Hence, the blocks containing pixels of salient region are discarded by judging whether there is a pixel of 0. Noise modeling operation is carried out in the remaining blocks.

Step 3: Calculation of noise estimator: For each retained block, noise of background region is fit by the alpha-stable

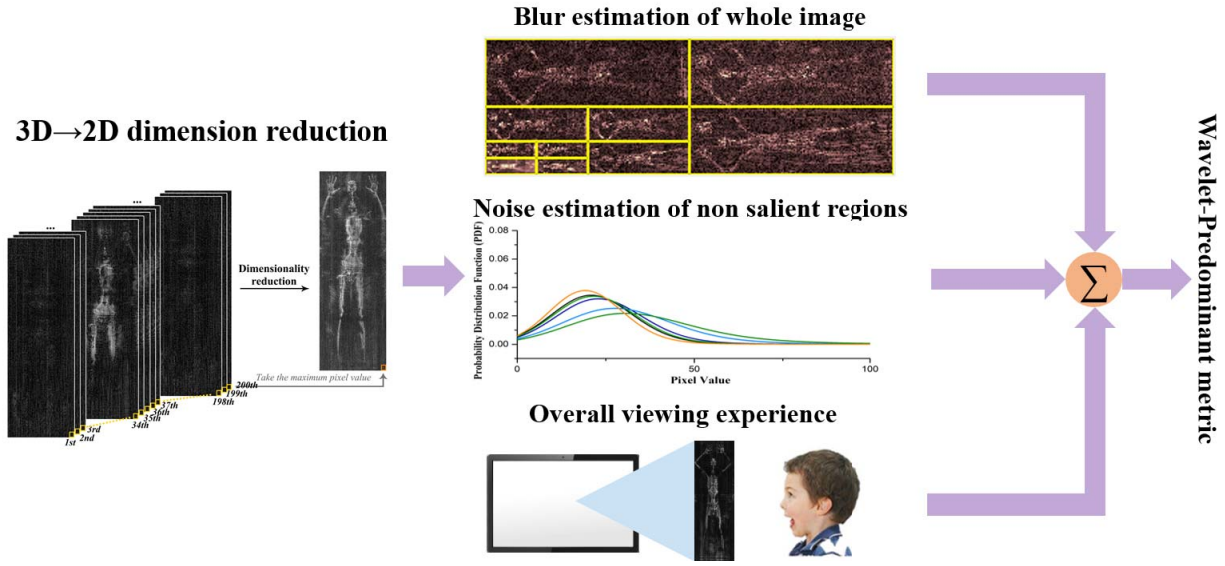

Fig. 7. Outline of wavelet-predominant algorithm for THz security images.

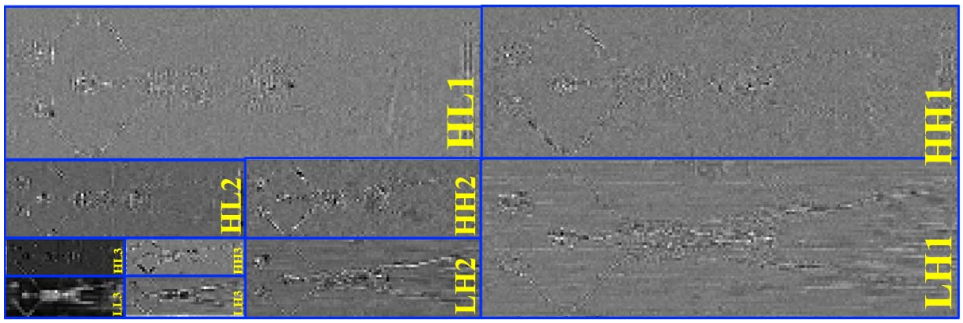

Fig. 8. Results of three-level separable discrete wavelet transform for THz security images.

model [33]. The characteristic function of alpha-stable model is defined as:

$$\phi(t;\alpha,\beta,\gamma,\delta) = e^{it\delta-|\gamma t|^{\alpha}(1-i\beta sgn(t)\varphi)} \tag{7}$$

where

$$\varphi = \begin{cases} \tan(\pi\alpha/2), & \alpha \neq 1 \\ (-2/\pi)\log|\gamma t|, & \alpha = 1 \end{cases} \tag{8}$$

α, β, γ and δ are stability, skewness, scale and location of the alpha-stable model respectively. In this study, two parameters viz. scale and location show the good performance for quality evaluation of THz security image. The noise estimator NS is computed via

$$NS = (1/N)\sum_{1}^{N}(a\alpha_n + b\beta_n + c\gamma_n + d\delta_n) \tag{9}$$

where N is the number of remaining image blocks; a, b, c and d is the coefficients for α, β, γ and δ, respectively. For this THz security image dataset, a, b and c are set to 0, and d is set as 1.

C. Overall Viewing Experience Estimator

In limited viewing time during the subjective evaluation, we consider that the fixation area of observers may be mainly on the salient region. So only viewing experience of saliency map is computed. To obtain the overall viewing experience estimator, the internal free-energy generative model $\mathcal{G}$ for visual perception is assumed to be parametric. This indicates that the model $\mathcal{G}$ is capable of explaining visual scenes by adjusting the parameter vector ψ. An essential premise in the free-energy principle is that the cognitive process is governed by the internal free-energy generative model $\mathcal{G}$ in human brain. If human brain receives a surprise, the brain will initiatively predict the meaningful information and remove residual uncertainty for explaining sensations with the model $\mathcal{G}$. Hence, given the saliency map I_s of THz security image I, the surprise of I_s can be measured by the integration of the joint distribution $P(I_s, \psi|\mathcal{G})$:

$$-\log P(I_s|\mathcal{G}) = -\log\int P(I_s,\psi|\mathcal{G})d\psi \tag{10}$$

A dummy term $Q(\psi|I_s,\mathcal{G})$ is introduced into both numerator and denominator of equation (10), and then the equation is altered using Jensen's inequality:

$$-\log P(I_s) \leq -\int Q(\psi|I_s,\mathcal{G})\log(P(I_s,\psi|\mathcal{G})/Q(\psi|I_s,\mathcal{G}))d\psi \tag{11}$$

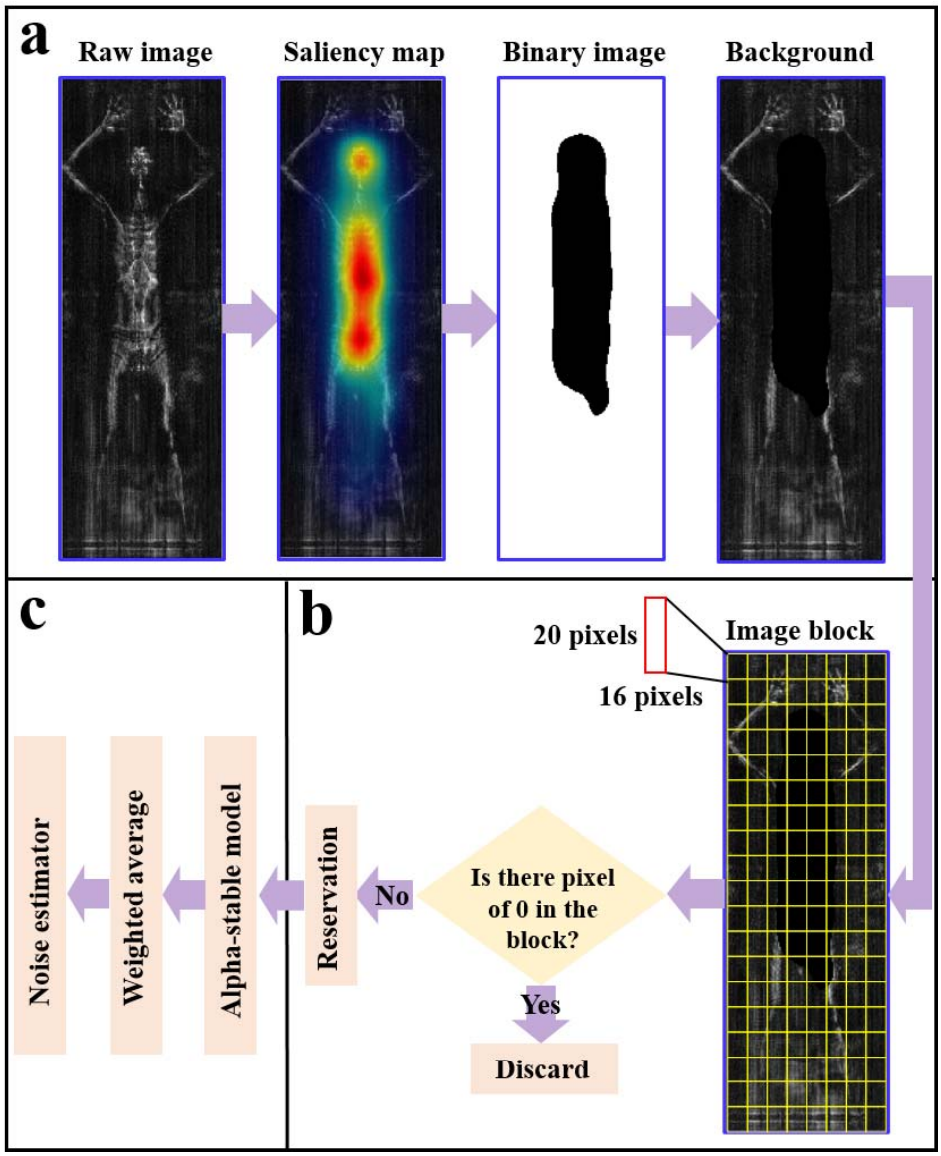

Fig. 9. Illustration of primary flowchart for the calculation of noise estimator: (a) detection of saliency map; (b) extraction of image block; and (c) calculation of parameters in alpha-stable model.

In the light of statistical physics and thermodynamics [34], the free energy of I_s is defined:

$$F(\psi) = -\int Q(\psi|I_s, \mathcal{G}) \log(P(I_s, \psi|\mathcal{G})/Q(\psi|I_s, \mathcal{G}))d\psi \tag{12}$$

Examining equation (11) and (12), we can find that $F(\psi)$ is an upper bound of "surprise" for image I_s. Notice that $P(I_s, \psi) = P(\psi|I_s)P(I_s)$, the equation (12) can be rewritten as:

$$F(\psi) = -\log P(I_s) + \mathbf{KL}(Q(\psi|I_s)||P(\psi|I_s)) \tag{13}$$

here $\mathbf{KL}(\cdot)$ represents the Kullback-Leibler divergence between the approximate posterior distribution $Q(\psi|I_s, \mathcal{G})$ and the true posterior distribution $P(\psi|I_s, \mathcal{G})$.

$F(\psi)$ can be approximated by the use of the linear auto-regressive approach.

D. Aggregate Wavelet-Predominant Estimator

The following equation is applied for combining these three estimators above mentioned to yield the aggregate wavelet-predominant estimator AW:

$$AW = aFISH + bNS + cF \tag{14}$$

where the parameters $a = 0.6$, $b = 0.2$, $c = 0.2$ are chosen empirically to assign the greater weight to the FISH estimator. The selection of weight is based on the distortion analysis of THz image. We argue that the possible ratio of sharpness, noise, human perception is 3:1:1 when measuring the quality of THz images.

IV. Statistical Analysis

In the current work, a total of seven opinion-unaware approaches viz. FISBLIM [35], SISBLIM [36], NIQE [13],

CPBD [37], SINE [38], S3 [39] and FISH [28] are executed for comparison. In order to calculate the performance metrics, the monotonic logistic function of five parameters $\{\beta_1, \beta_2, \beta_3, \beta_4, \beta_5\}$ is leveraged to fit the MOSs estimated by objective IQA algorithm, and the equation below was afterwards used to map the fitted objective scores to the subjective scores.

$$\textit{Mapped Quality}(x) = \beta_1\Big(1/2 - 1/\Big(1 + e^{\beta_2(x-\beta_3)}\Big)\Big) + \beta_4 x + \beta_5 \tag{15}$$

where *Mapped Quality* and x are the mapped objective score and its original score, respectively.

For quantitative analysis, three metrics viz., Pearson Linear Correlation Coecient (PLCC), Spearman Rank-Order Correlation Coefficient (SROCC) and Root Mean Squared Error (RMSE) are used to examine the performance of IQA algorithms on THz security images. The definitions of these metrics are below:

$$SRCC = 1 - \frac{6\sum_{n=1}^{N} d_i^2}{N\big(N^2-1\big)} \tag{16}$$

$$PLCC = \frac{\sum_{i=1}^{N}(p_i - \bar{p})(s_i - \bar{s})}{\sqrt{\sum_{i=1}^{N}(p_i - \bar{p})^2 (s_i - \bar{s})^2}} \tag{17}$$

$$RMSE = \sqrt{\frac{1}{N}\sum_{i=1}^{N}(p_i - s_i)^2} \tag{18}$$

here d_i denotes the difference between the subjective and objective scores of ith images, and N represents the number of testing images. In addition, s_i and p_i are the subjective (reference) scores and objective (predicted) scores of the ith image after nonlinear regression. $\bar{s}$ and $\bar{p}$ are the average of all s_i and p_i, respectively. Specifically, SRCC indicates the prediction monotonicity, PLCC reflects the prediction accuracy and RMSE represents the prediction consistency. An excellent IQA metric is expected to obtain the SRCC and PLCC close to 1, yet the value near 0 for RMSE.

Besides, the linear correlation plot and the Bland-Altman plot [40] are further used to check the effectiveness of IQA algorithms and visualize the distribution of predicted data.

For usability evaluation, we use four metrics namely accuracy, precision, recall rate and false positive rate to estimate the model performance, thus evaluating the effectiveness of IQA measures used. These four metrics are calculated using the following equations:

$$Accuracy = \frac{tp + tn}{tp + tn + fp + fn} \tag{19}$$

$$Precision = \frac{tp}{tp + fp} \tag{20}$$

$$Recall = \frac{tp}{tp + fn} \tag{21}$$

$$False\ positive\ rate = \frac{fp}{tn + fp} \tag{22}$$

where if the sample is positive and the predicted class is positive, it is counted as true positives (*tp*); if the predicted class is negative, it is grouped as false negatives (*fn*). If the negative sample is classified as negative, it is counted as true negatives (*tn*); otherwise counted as false positives (*fp*).

TABLE II
PERFORMANCE COMPARISON OF THE PROPOSED METRICS AND OTHER OPINION-UNAWARE BLIND IQA METHODS FOR THZ SECURITY IMAGE. (THE SUPERIOR RESULTS ARE HIGHLIGHTED IN BOLDFACE)

Criterion	Estimator	PLCC	SROCC	RMSE
FISBLIM	*ss*	0.551	0.450	0.739
SISBLIM	*score3*	**0.827**	0.798	0.497
NIQE	*quality*	0.445	0.403	0.793
S3	*s31*	**0.872**	0.856	0.434
CPBD	$metric_{cpbd}$	0.205	0.112	0.866
SINE	$noise_{SD}$	0.346	0.391	0.831
FISH	*sh1*	**0.893**	**0.871**	**0.399**
Noise estimator	*NS*	**0.852**	0.828	0.463
Aggregate estimator	*AW*	**0.900**	**0.873**	**0.386**

V. EXPERIMENTAL RESULTS AND ANALYSIS

A. No-Reference IQA for THz Security Image

The statistical data regarding the performance of seven opinion-unaware no-reference IQA methods is presented in Table II.

As shown in Table II, NIQE, FISBLIM, CPBD and SINE result in low PLCC (SROCC) and high RMSE values for the assessment of THz security image quality (below 0.5600 (0.4600) and beyond 0.7300, respectively). It is not surprising that these general-purpose no-reference IQA algorithms work not so well for THz security images. Since those algorithms were implicitly designed for natural images, especially these natural scene statistics (NSS) based methods. In contrast, THz security images largely deviate from NSS. It can be observed that SISBLIM works relatively well with PLCC (SROCC) and RMSE values of 0.827 (0.798) and 0.497. The possible reason for this is: SISBLIM is a six-step blind metric which integrates joint effects of different distortion sources into one metric, and one module in SISBLIM may be sensitive to quality of THz security image. Two sharpness algorithms viz. S3 and FISH are promising for the estimation of THz security images with PLCC (SROCC) values of 0.872 (0.856) and 0.893 (0.871), and with RMSE values of 0.434 and 0.399. In comparison, FISH achieves the slightly superior overall performance to S3. As illustrated in Fig. 5, it can be found that high-quality THz security images have clean backgrounds, and the whole image is relatively smooth except for the target. Nonetheless, in terms of THz images of low quality, the whole image is quite noisy and sharp. Therefore, sharpness algorithms will give low quality scores for THz security images of high quality and high quality scores for THz security images of low quality (data not shown), which is contrary to natural images. This reversed phenomenon has no effect on the final predictive ability of sharpness algorithm. The noise estimator predicts quality of THz security image with PLCC (SROCC) and RMSE values of 0.852 (0.828) and 0.463, whose performance is slightly inferior to these of S3 and FISH. The good estimation of noise estimator indicates that the noisy pattern of THz security image indeed follows the alpha-stable distribution [29]. The aggregate wavelet-predominant estimator gives the best

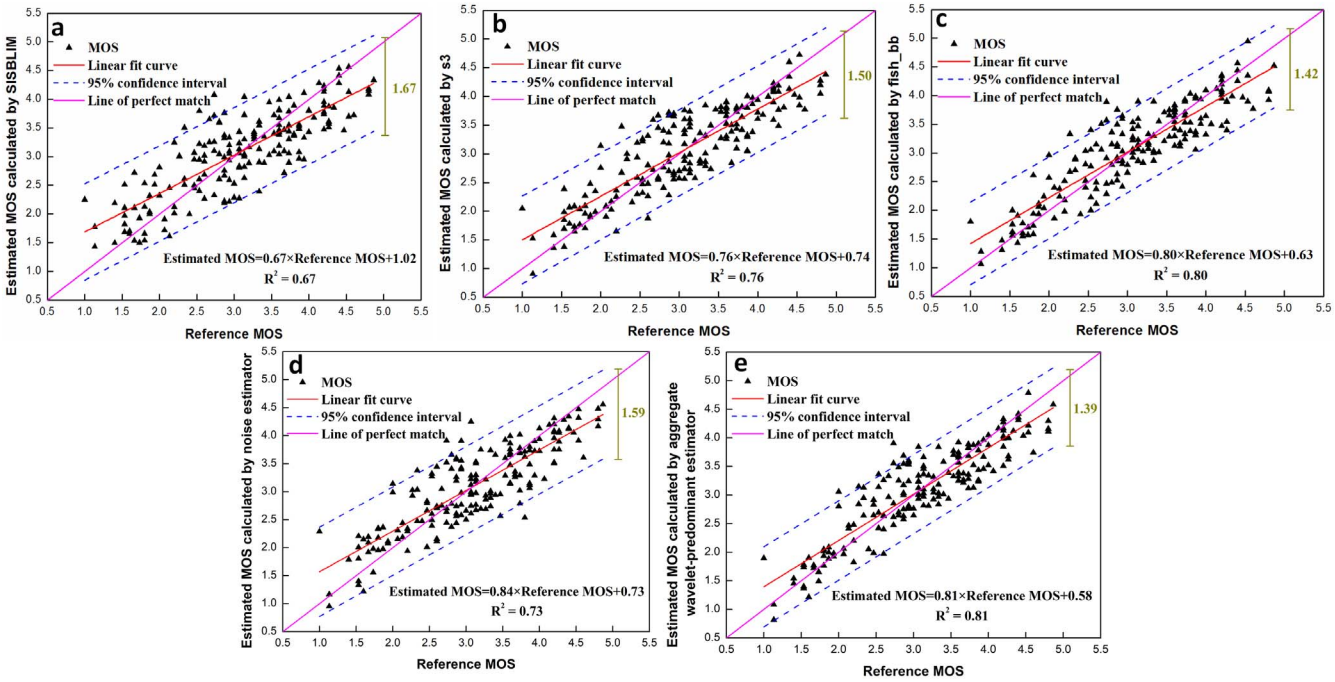

Fig. 10. Scatter plots and linear regressions of reference MOSs versus predicted quality using SISBLIM (a), S3 (b), FISH (c), noise estimator (d) and aggregate wavelet-predominant estimator (e).

prediction than other no-reference IQA approaches for assessing THz image quality, with PLCC (SROCC) values of 0.900 (0.873), and with RMSE value of 0.386.

Fig. 10 visualizes the distributions of the estimated and reference MOSs. As shown in Fig. 10, with respect to SISBLIM, S3, FISH, noise estimator and aggregate estimator, the scatter plots of predicted against reference MOSs clearly reveal that a majority of the THz image samples are mainly close to the line of perfect match (slope = 1) and within the 95% confidence intervals. The vertical distances between the upper and lower 95% confidence intervals are 1.67, 1.50, 1.42, 1.59 and 1.39 for SISBLIM, S3, FISH, noise estimator and aggregate estimator, respectively, suggesting that the aggregate estimator performs better than other algorithms for THz security images. In respect to linear regression analysis, the proposed aggregate estimator is further verified to outperform SISBLIM, S3, FISH and noise estimator with determination coefficients (R^2) of 0.81 versus 0.67, 0.76, 0.80 and 0.73.

Fig. 11 demonstrates the Bland-Altman plot of reference and estimated MOSs. We can see that the distribution of points in Bland-Altman plot in Fig. 11 is quite similar to that in Fig. 10. For the Bland-Altman plot, it is generally believed that the points in limits of agreement range account for 95% of all points, and these two methods are considered to be in good agreement and interchangeable. For these three approaches, the majority of points are dispersed around the line of perfect agreement. In Fig. 11, approximately 92.8% of data points estimated by FISH locate within the limits of agreement of 0.7848 and 0.7848. In contrast, approximately 94.5% of data points estimated by noise estimator and aggregate wavelet-predominant estimator locate within the limits of agreement. This suggests that the noise estimator and aggregate wavelet-predominant estimator outperform the FISH method. Considering the degree of aggregation of data points, the aggregate wavelet-predominant estimator yields the better performance than the noise estimator, with the upper limits of agreement of 0.7582 versus 0.9105. Hence, the aggregate wavelet-predominant estimator can substitute for the subjective IQA of THz security image.

B. Usability Identification of THz Security Images

Currently, THz images have been widely used in many application scenarios and the identification of their usability will become a broad and fundamental problem. THz image usability assessment is a prerequisite for all subsequent image processing and analysis operations. Accurate definition of THz image usability is: an indicator that estimates the maximum allowable image distortion. To some extent, image quality metrics can be used as indicators to measure the image usability.

Because THz imaging equipment is relatively expensive, many investigators in image quality evaluation research domain have difficulty accessing THz images. Based on results of preliminary literature research, there is no research on the usability evaluation of THz images, especially for THz security images. Compared to images of other specific image modalities, the quality of THz security images is more closely related to the performance (such as the detection accuracy of contraband) of the final commercial system. In summary, the usability identification of THz security images has very important application value, which can effectively guide the development of THz image processing software and optimize

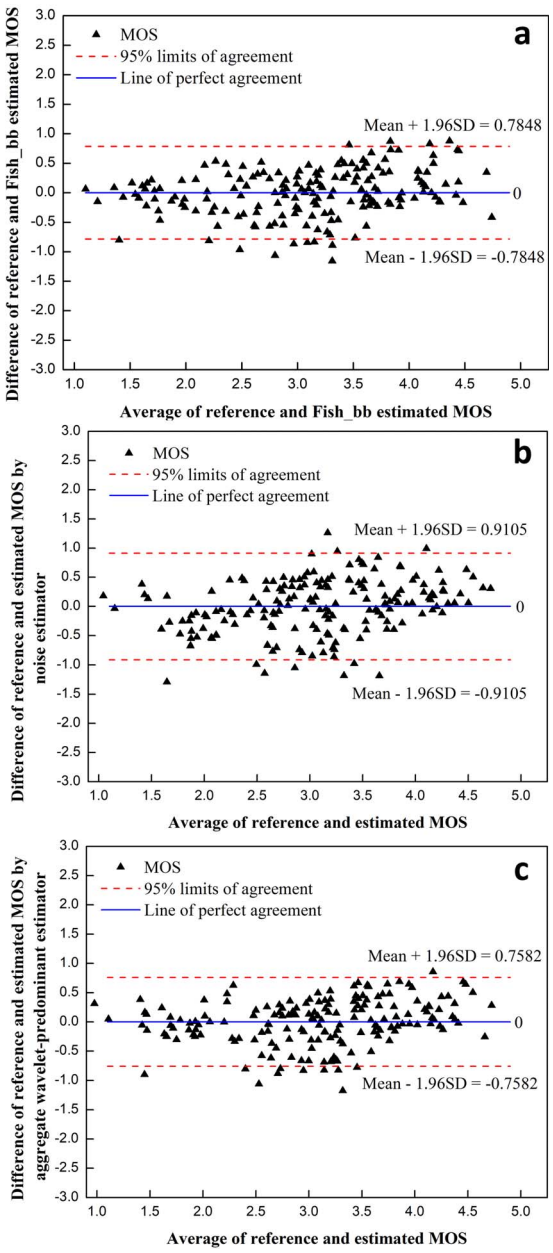

Fig. 11. Bland-Altman plot ($N = 181$ images) of the difference against average for THz IQA using subjective evaluation and objective IQA algorithms: FISH (a), noise estimator (b) and aggregate wavelet-predominant estimator (c).

the design of the overall imaging system, thereby improving the detection accuracy of contraband.

Table III summarizes the unsupervised classication results of usability identification for THz security images based on five IQA algorithms. The five IQA algorithms viz. SISBLIM, S3, FISH, noise estimator and aggregate estimator achieve the overall classification accuracies of 76.8%, 80.1%, 84.0%, 79.6% and 84.0%, respectively. Among them, the aggregate estimator and FISH produce the highest accuracy values. Checking other performance metrics, the aggregate estimator and FISH also give the satisfactory performance, with precision (recall) of 79.8% (95.0%) and 78.9% (97.0%), with fp rate of 29.6% and 32.1%, respectively. Prediction denotes that how many samples predicted to be positive are correct.

TABLE III
RESULTS OF USABILITY IDENTIFICATION FOR THZ SECURITY IMAGES USING FIVE IQA FEATURES

IQA measure	Performance metric			
	Accuracy	*Precision*	*Recall*	*Fp rate*
SISBLIM	0.768	0.746	0.880	0.370
S3	0.801	0.814	0.830	0.235
FISH	0.840	0.789	0.970	0.321
Noise estimator	0.796	0.789	0.860	0.284
Aggregate estimator	0.840	0.798	0.950	0.296

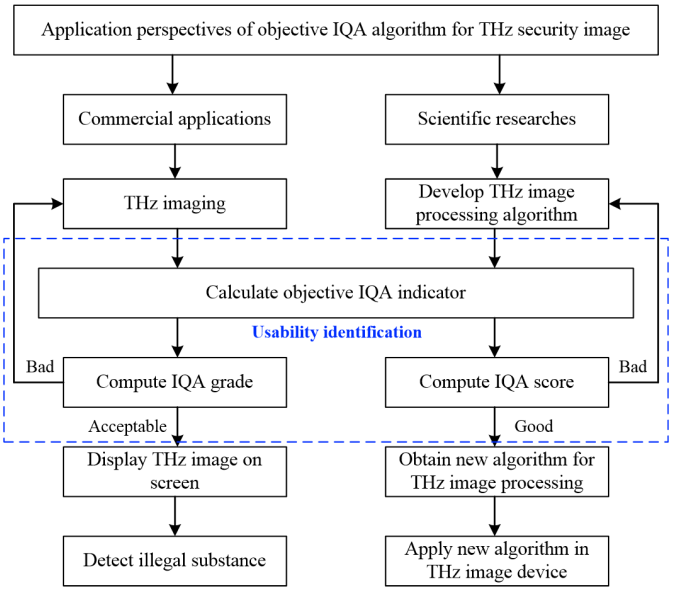

Fig. 12. Role of THz IQA algorithms in the overall THz security imaging system.

Recall rate indicates how many positive samples in sample set are correctly predicted. Fp rate represents the probability of dividing true negative samples into positive samples. Although S3 has the relatively high prediction and low fp rate, its accuracy and recall rate are inferior to these of aggregate estimator, with nearly 4% and 12% decrement, respectively.

C. Application Perspectives and Further Research Tendency

The possible application perspectives of the IQA of THz image quality can refer to commercial applications and scientific researches. For commercial applications, as shown in Fig. 12, with the help of the IQA indicator, THz security images of good quality can be displayed on the screen via reshoot or shooting parameters reset. With respect to scientific researches, we can use the IQA indicator as a criterion to assist in developing new THz security image processing algorithms such as THz image enhancement for THz imaging device (Fig. 12).

FISH algorithm takes the majority of the weight in this integrated algorithm. The possible reason for good performance of FISH algorithm is listed below: high-quality THz security images have clean background, and the whole image is relatively smooth except for the target. For THz images of low quality, the whole image is quite noisy and sharp. Consequently, sharpness algorithms can have low quality

scores for THz images of high quality and high quality scores for THz images of low quality (data not shown), which is contrary to natural images. This reversed phenomenon has no effect on the final predictive ability of sharpness algorithm.

According to the description of Section II-B, the THz security image is three-dimensional. Therefore, we are not sure that whether the THz display mode used in this work is better than the other display modes or not. For example, we can also use the cross profile of maximum average pixel intensity or the averaging the highest 10% pixel values in Z direction to be displayed in the viewing screen for security staffs. In addition, nowadays, THz-related acquisition devices are somewhat confidential. Hence, different devices and imaging modes will create different types of THz images. There is a great possibility that this algorithm will fail in other THz acquisition devices. Cross-device and cross-modal adaptive algorithms are difficult to be developed unless there is a relatively uniform standard for future THz data acquisition devices.

The proposed algorithm is problematic in its universality. Yet this is a new attempt and also a process of exploration for THz security image quality assessment and usability identification. The reasons are listed as follows: 1) the existing THz image quality evaluation library is not yet available, and we currently use the self-built THz image quality library to discuss the feasibility of the quality evaluation algorithm in the field of THz image quality evaluation; 2) as far as we know, the THz images obtained by different THz devices or the same device in different parameters are extremely different. Unlike natural images, THz images do not currently have any standardized acquisition device or acquisition standard; 3) different subjective evaluation standards will get different MOS values, thus making the corresponding analysis invalid. In preliminary experiment, we have designed two other subjective experiments based on the single-stimulus approach to evaluate the global impairment and the local clarity of body and contraband, respectively. However, almost all the image quality evaluation algorithms are invalid on these two MOS vectors; and 4) the structure of raw THz data is three-dimensional. Therefore, for the same THz imaging device, different two-dimensional display modes will let subjective evaluators to derive different MOS values. In order to solve these problems (these problems may not have a standard solution), we have released raw THz data for other research investigators (https://doi.org/10.6084/m9.figshare.7700123.v3). Possible researches on this dataset may include the development of THz quality standards, the selection of the best display mode, the enhancement of images, the modeling of image noise, and the detection of prohibited goods.

Thus, there exist two possible research tendencies for the further study: 1) devise a rule (this rule may be an IQA algorithm) to confirm one best display mode of THz security image for both commercial applications and scientific researches; and 2) design a series of IQA approaches including opinion-aware no-reference models for quality assessment and usability identification of THz security image, and these algorithms may be developed on the basis of three-dimensional or two-dimensional THz security images.

VI. Conclusion

In this paper, we present the aggregate wavelet-predominant estimator without any training procedures to conduct the quality assessment and usability identification of THz security image. The performance of aggregate wavelet-predominant estimator is validated on the self-built THz security image dataset. For quantitative quality evaluation, the aggregate wavelet-predominant estimator can predict the MOS values of THz security images with PLCC, SROCC and RMSE of 0.900, 0.873 and 0.386, respectively, whose performance is superior to these of other opinion-unaware approaches, namely FISBLIM, SISBLIM, NIQE, CPBD, SINE, S3, FISH and noise estimator. The R^2 of linear regression of reference MOSs versus estimated quality using the proposed estimator is 0.81. The result of Bland-Altman analysis further verifies that the aggregate wavelet-predominant estimator can substitute for the subjective IQA of THz security image, with approximately 94.5% of data points locating within the limits of agreement. In terms of usability identification, the wavelet-predominant estimator produces the promising results, with accuracy, precision, recall rate, fp rate of 84.0%, 79.8%, 95.0% and 29.6%, respectively. Moreover, the possible application perspectives are discussed: 1) for commercial applications, we can guarantee THz security images of good quality. When the acquired image owns the unacceptable IQA value, the imaging system can automatically reshoot by adjusting shooting parameters; and 2) for scientific researches, the IQA metric can be used to assist in designing the new THz security image analysis algorithms.

References

[1] M. Tonouchi, "Cutting-edge terahertz technology," *Nat. Photon.*, vol. 1, no. 2, pp. 97–105, 2007.

[2] C. Sirtori, "Applied physics: Bridge for the terahertz gap," *Nature*, vol. 417, no. 6885, pp. 132–133, 2002.

[3] D. Saeedkia, *Handbook of Terahertz Technology for Imaging, Sensing and Communications*. Amsterdam, The Netherlands: Elsevier, 2013.

[4] K.-J. Mu, Z.-W. Zhang, and C.-L. Zhang, "Terahertz science and technology," *J. China Acad. Electron. Inf. Technol.*, vol. 4, no. 3, pp. 221–230, 2009.

[5] K. A. Moldosanov, A. V. Postnikov, V. M. Lelevkin, and N. J. Kairyev, "Terahertz imaging technique for cancer diagnostics using frequency conversion by gold nano-objects," *Ferroelectrics*, vol. 509, no. 1, pp. 158–166, 2017.

[6] S.-H. Park, W.-H. Chung, and H.-S. Kim, "Non-contact measurement of the electrical conductivity and coverage density of silver nanowires for transparent electrodes using terahertz spectroscopy," *Meas. Sci. Technol.*, vol. 28, no. 2, 2016, Art. no. 025001.

[7] J. F. Federici *et al.*, "Thz imaging and sensing for security applications—Explosives, weapons and drugs," *Semicond. Sci. Technol.*, vol. 20, no. 7, p. S266, 2005.

[8] L. Hou, X. Lou, Z. Yan, H. Liu, and W. Shi, "Enhancing terahertz image quality by finite impulse response digital filter," in *Proc. 39th Int. Conf. Infrared Millimeter Terahertz Waves (IRMMW-THz)*, 2014, pp. 1–2.

[9] A. J. Fitzgerald *et al.*, "Evaluation of image quality in terahertz pulsed imaging using test objects," *Phys. Med. Biol.*, vol. 47, no. 21, pp. 3865–3873, 2002.

[10] H. R. Sheikh, M. F. Sabir, and A. C. Bovik, "A statistical evaluation of recent full reference image quality assessment algorithms," *IEEE Trans. Image Process.*, vol. 15, no. 11, pp. 3440–3451, Nov. 2006.

[11] Z. Wang, A. C. Bovik, H. R. Sheikh, and E. P. Simoncelli, "Image quality assessment: From error visibility to structural similarity," *IEEE Trans. Image Process.*, vol. 13, no. 4, pp. 600–612, Apr. 2004.

[12] K. Gu *et al.*, "Blind quality assessment of tone-mapped images via analysis of information, naturalness, and structure," *IEEE Trans. Multimedia*, vol. 18, no. 3, pp. 432–443, Mar. 2016.

[13] A. Mittal, R. Soundararajan, and A. C. Bovik, "Making a 'completely blind' image quality analyzer," *IEEE Signal Process. Lett.*, vol. 20, no. 3, pp. 209–212, Mar. 2013.
[14] K. Gu, G. Zhai, X. Yang, and W. Zhang, "Using free energy principle for blind image quality assessment," *IEEE Trans. Multimedia*, vol. 17, no. 1, pp. 50–63, Jan. 2015.
[15] W. Xue, X. Mou, L. Zhang, A. C. Bovik, and X. Feng, "Blind image quality assessment using joint statistics of gradient magnitude and Laplacian features," *IEEE Trans. Image Process.*, vol. 23, no. 11, pp. 4850–4862, Nov. 2014.
[16] A. K. Moorthy and A. C. Bovik, "Blind image quality assessment: From natural scene statistics to perceptual quality," *IEEE Trans. Image Process.*, vol. 20, no. 12, pp. 3350–3364, Dec. 2011.
[17] A. Mittal, A. K. Moorthy, and A. C. Bovik, "No-reference image quality assessment in the spatial domain," *IEEE Trans. Image Process.*, vol. 21, no. 12, pp. 4695–4708, Dec. 2012.
[18] M. A. Saad, A. C. Bovik, and C. Charrier, "Blind image quality assessment: A natural scene statistics approach in the DCT domain," *IEEE Trans. Image Process.*, vol. 21, no. 8, pp. 3339–3352, Aug. 2012.
[19] L. S. Chow and R. Paramesran, "Review of medical image quality assessment," *Biomed. Signal Process. Control*, vol. 27, pp. 145–154, May 2016.
[20] J. Long and S. Li, "Near infrared face image quality assessment system of video sequences," in *Proc. 6th Int. Conf. Image Graph. (ICIG)*, 2011, pp. 275–279.
[21] W. Wu, G. Liu, Z. Zhou, and Z. Gu, "Image quality assessment software of security screening system," in *Proc. 42nd Annu. IEEE Int. Carnahan Conf. Security Technol. (ICCST)*, 2008, pp. 107–111.
[22] J. Irvine, M. Young, S. German, and R. Eaton, "Perceived X-ray image quality for baggage screening," in *Proc. IEEE Appl. Imagery Pattern Recognit. Workshop (AIPR)*, 2015, pp. 1–9.
[23] J. Galbally, S. Marcel, and J. Fierrez, "Image quality assessment for fake biometric detection: Application to iris, fingerprint, and face recognition," *IEEE Trans. Image Process.*, vol. 23, no. 2, pp. 710–724, Feb. 2014.
[24] P. Pravallika and K. S. Prasad, "SVM classification for fake biometric detection using image quality assessment: Application to iris, face and palm print," in *Proc. Int. Conf. Inventive Comput. Technol. (ICICT)*, vol. 1, 2016, pp. 1–6.
[25] S. Saranya, S. V. Sherline, and M. Maheswari, "Fake biometric detection using image quality assessment: Application to iris, fingerprint recognition," in *Proc. 2nd Int. Conf. Sci. Technol. Eng. Manag. (ICONSTEM)*, 2016, pp. 98–103.
[26] M. Hu *et al.*, "Terahertz security image quality assessment by no-reference model observers," in *Proc. Int. Forum Digit. TV Wireless Multimedia Commun.*, 2017, pp. 100–114.
[27] "Methodology for the subjective assessment of the quality of television pictures," Int. Telecommun. Union, Geneva, Switzerland, ITU-Recommendation BT 500-11, 2015.
[28] P. V. Vu and D. M. Chandler, "A fast wavelet-based algorithm for global and local image sharpness estimation," *IEEE Signal Process. Lett.*, vol. 19, no. 7, pp. 423–426, Jul. 2012.
[29] Z. Wang, M. Hu, E. E. Kuruoglu, W. Zhu, and G. Zhai, "How do detected objects affect the noise distribution of terahertz security images?" *IEEE Access*, vol. 6, pp. 41087–41092, 2018.
[30] G. Zhai, X. Wu, X. Yang, W. Lin, and W. Zhang, "A psychovisual quality metric in free-energy principle," *IEEE Trans. Image Process.*, vol. 21, no. 1, pp. 41–52, Jan. 2012.
[31] A. Cohen, I. Daubechies, and J.-C. Feauveau, "Biorthogonal bases of compactly supported wavelets," *Commun. Pure Appl. Math.*, vol. 45, no. 5, pp. 485–560, 1992.
[32] J. Harel, C. Koch, and P. Perona, "Graph-based visual saliency," in *Proc. Adv. Neural Inf. Process. Syst.*, 2007, pp. 545–552.
[33] G. R. Arce, *Nonlinear Signal Processing: A Statistical Approach*. Hoboken, NJ, USA: Wiley, 2005.
[34] R. Feynman, *Statistical Mechanics: A Set of Lectures (Advanced Book Classics)*. Boulder, CO, USA: Westview, 1998.
[35] K. Gu *et al.*, "FISBLIM: A five-step blind metric for quality assessment of multiply distorted images," in *Proc. Workshop Signal Process. Syst. (SiPS)*, 2013, pp. 241–246.
[36] K. Gu, G. Zhai, X. Yang, and W. Zhang, "Hybrid no-reference quality metric for singly and multiply distorted images," *IEEE Trans. Broadcast.*, vol. 60, no. 3, pp. 555–567, Sep. 2014.
[37] N. D. Narvekar and L. J. Karam, "A no-reference image blur metric based on the cumulative probability of blur detection (CPBD)," *IEEE Trans. Image Process.*, vol. 20, no. 9, pp. 2678–2683, Sep. 2011.
[38] D. Zoran and Y. Weiss, "Scale invariance and noise in natural images," in *Proc. IEEE 12th Int. Conf. Comput. Vis.*, 2009, pp. 2209–2216.
[39] C. T. Vu, T. D. Phan, and D. M. Chandler, "S_3: A spectral and spatial measure of local perceived sharpness in natural images," *IEEE Trans. Image Process.*, vol. 21, no. 3, pp. 934–945, Mar. 2012.
[40] A. Carkeet and Y. T. Goh, "Confidence and coverage for Bland–Altman limits of agreement and their approximate confidence intervals," *Stat. Methods Med. Res.*, vol. 27, no. 5, pp. 1559–1574, 2018.

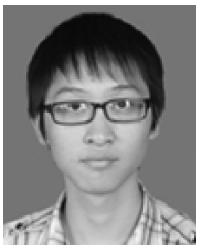

Menghan Hu received the Ph.D. degree (Hons.) in biomedical engineering from the University of Shanghai for Science and Technology in 2016. From 2016 to 2018, he was a Post-Doctoral Researcher with Shanghai Jiao Tong University. He is currently an Associate Professor with the Shanghai Key Laboratory of Multidimensional Information Processing, East China Normal University.

Guangtao Zhai (M'10) received the B.E. and M.E. degrees from Shandong University, Shandong, China, in 2001 and 2004, respectively, and the Ph.D. degree from Shanghai Jiao Tong University, Shanghai, China, in 2009, where he is currently a Research Professor with the Institute of Image Communication and Information Processing. From 2006 to 2007, he was a Student Intern with the Institute for Infocomm Research, Singapore. From 2007 to 2008, he was a visiting student with the School of Computer Engineering, Nanyang Technological University, Singapore. From 2008 to 2009, he was a visiting student with the Department of Electrical and Computer Engineering, McMaster University, Hamilton, ON, Canada, where he was a Post-Doctoral Fellow from 2010 to 2012. From 2012 to 2013, he was a Humboldt Research Fellow with the Institute of Multimedia Communication and Signal Processing, Friedrich Alexander University of Erlangen–Nuremberg, Germany. His research interests include multimedia signal processing and perceptual signal processing. He was a recipient of the National Excellent Ph.D. Thesis from the Ministry of Education of China in 2012.

Rong Xie received the bachelor's and master's degrees in electrical engineering from Northeast Dianli University, Jilin City, China, in 1996 and 1999, respectively, and the Ph.D. degree in electrical engineering from Zhejiang University in 2002. She joined Shanghai Jiao Tong University in 2002 as an Assistant Professor. She is currently an Associate Professor with the Cooperative Medianet Innovation Center, Shanghai Jiao Tong University. In 2009, she visited the Information Laboratory, Computer Science Department, University of Southern California, USA, as a Visiting Scholar for seven months. From 2009 to 2010, she was a Supervisor with the IT Center of Shanghai World Expo Coordination Bureau. She received National Natural Science Fund in 2010 and Innovation fund of aerospace science and technology in 2005. She has published 40 refereed papers, and has filed 11 patents. Her research interests are in the areas of video coding and video processing. She was a recipient of the Best Paper Award from IEEE BMSB 2015. She is a member of IEEE Signal Processing Society.

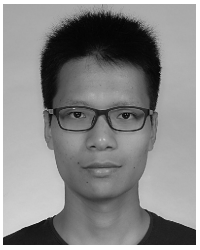

Xiongkuo Min received the B.E. degree in electronic engineering from Wuhan University, Wuhan, China, in 2013. He is currently pursuing the Ph.D. degree with the Institute of Image Communication and Network Engineering, Shanghai Jiao Tong University, Shanghai, China. From 2016 to 2017, he was a visiting student with the Department of Electrical and Computer Engineering, University of Waterloo, Canada. His research interests include image/video quality assessment, visual attention modeling, and perceptual signal processing. He was a recipient of the Best Student Paper Award of ICME 2016.

Qingli Li received the B.S. and M.S. degrees in computer science and engineering from Shandong University, Jinan, China, in 2000 and 2003, respectively, and the Ph.D. degree in pattern recognition and intelligent system from Shanghai Jiaotong University, Shanghai, China, in 2006. He is currently a Professor with the Shanghai Key Laboratory of Multidimensional Information Processing, East China Normal University, Shanghai, where he is researching on medical imaging, pattern recognition, and image processing.

Xiaokang Yang (M'00–SM'04–F'18) received the B.S. degree from Xiamen University, Xiamen, China, in 1994, the M.S. degree from the Chinese Academy of Sciences, Shanghai, China, in 1997, and the Ph.D. degree from Shanghai Jiao Tong University, Shanghai, in 2000.

He is currently a Distinguished Professor with the School of Electronic Information and Electrical Engineering, and the Deputy Director of the Institute of Image Communication and Information Processing, Shanghai Jiao Tong University. From 2000 to 2002, he was a Research Fellow with the Centre for Signal Processing, Nanyang Technological University, Singapore. From 2002 to 2004, he was a Research Scientist with the Institute for Infocomm Research, Singapore. From 2007 to 2008, he visited the Institute for Computer Science, University of Freiburg, Freiburg im Breisgau, Germany, as an Alexander von Humboldt Research Fellow. He has published over 200 refereed papers, and has filed 60 patents. His current research interests include image processing and communication, computer vision, and machine learning.

Prof. Yang is an Associate Editor of the IEEE TRANSACTIONS ON MULTIMEDIA and a Senior Associate Editor of the IEEE SIGNAL PROCESSING LETTERS. He was a Series Editor of Springer CCIS, and an Editorial Board Member of *Digital Signal Processing*. He is also the Chair of the Multimedia Big Data Interest Group of MMTC Technical Committee, IEEE Communication Society. He is a member of Asia–Pacific Signal and Information Processing Association, the VSPC Technical Committee of the IEEE Circuits and Systems Society, and the MMSP Technical Committee of the IEEE Signal Processing Society.

Wenjun Zhang (M'02–SM'10–F'12) received the B.S., M.S., and Ph.D. degrees in electronic engineering from Shanghai Jiao Tong University, Shanghai, China, in 1984, 1987, and 1989, respectively. From 1990 to 1993, he was a Post-Doctoral Fellow with Philips Kommunikation Industrie AG, Nuremberg, Germany, where he was actively involved in developing the HD-MAC system. He joined the Faculty Member of Shanghai Jiao Tong University, in 1993, and became a Full Professor with the Department of Electronic Engineering in 1995. He holds over 40 patents and authored or co-authored over 90 papers in international journals and conferences. His main research interests include digital video coding and transmission, multimedia semantic processing, and intelligent video surveillance. He is a Chief Scientist with the Chinese National Engineering Research Centre of Digital Television (DTV), an industry/government consortium in DTV technology research and standardization, and the Chair of the Future of Broadcast Television Initiative Technical Committee. As the National HDTV TEEG Project Leader, he successfully developed the first Chinese HDTV prototype system in 1998. He was one of the main contributors to the Chinese Digital Television Terrestrial Broadcasting Standard issued in 2006 and is leading team in designing the next generation of broadcast television system in China since 2011.